THE JOURNAL OF PHYSICAL CHEMISTRY C

Article

pubs.acs.org/JPCC

Patterning Gold Nanoparticle Using Scanning Electrochemical Microscopy

José M. Abad,*[†,‡] Álvaro Y. Tesio,[†,§] Félix Pariente,[†] and Encarnación Lorenzo[†,‡]

[†]Departamento de Química Analítica y Análisis Instrumental, Universidad Autónoma de Madrid, Cantoblanco, 28049 Madrid, Spain

[‡]Instituto Madrileño de Estudios Avanzados en Nanociencia (IMDEA-Nanociencia), Fáraday, 9, Campus UAM, Cantoblanco, 28049 Madrid, Spain

Supporting Information

ABSTRACT: Patterned arrays of gold nanoparticles (AuNPs) are prepared using scanning electrochemical microscopy by electrochemical reduction of a gold salt at a platinum ultramicroelectrode positioned on top of an unbiased gold surface, modified with a biphenyl dithiol self-assembled monolayer (SAM). The synthesized AuNPs are chemisorbed on the thiolated SAM, and by moving the microelectrode in a lateral direction across the surface while applying a reduction potential, particle-like lines are generated.

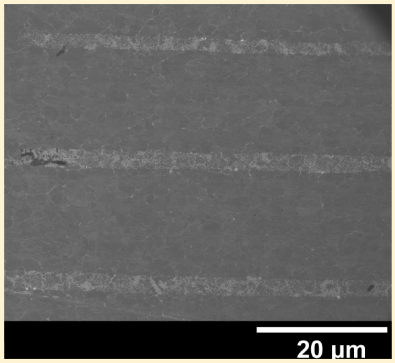

INTRODUCTION

Fabrication of patterned arrays of gold nanoparticles (AuNPs) have attracted a great deal of interest for many applications including catalysts,[1,2] sensors,[3] and electronic devices development,[4,5] due to their unusual particle-size-dependent optical, electrical, magnetic, and chemical properties.[6] Particle arrays can be prepared by different techniques and procedures, mainly by lithography,[7] including photolithography,[8−10] electron beam lithography,[11−14] dip-pen nanolithography,[15−17] soft lithography such as microcontact printing,[18,19] and nanoimprinting.[20] In addition, these have been fabricated by scanning-probe-based lithographies[21−29] (atomic force microscopy, scanning tunnel microscopy, scanning near-field optical microscopy, and scanning beam lithography) combined with the use of template self-assembly techniques from nanoparticles in solution.

Electrochemical particle synthesis and deposition using scanning electrochemical microscopy (SECM) offers an alternative approach for the formation of micrometer and submicrometer patterns of AuNPs on surfaces.[30,31] SECM has been shown to be a powerful tool for the deposition of metals on polymer films[32] and on either conducting[33,34] or nonconducting substrates.[35,36] Also, SECM has been employed in various ways for local deposition of metal NPs.[37−43] Typically, they follow a tip generation/substrate collection approach where a metal ultramicroelectrode placed in close proximity to a surface is anodically dissolved to electrogenerate a flux of metal ions that are further reduced after diffusion to the substrate resulting in the formation of nanoparticles. The reduction can be accomplished at an externally biased conductive substrate applying an appropriate reduction potential. Following this method, Mandler et al. locally deposited AuNPs onto silicon arranged in micropatterns from a gold UME.[39,42] This approach has been further extended to the nanoparticle deposition of other metals such as silver[44] and cobalt,[45] UME being made of the same metal, and to other surfaces (i.e., indium tin oxide)[37] and interfaces (i.e., liquid−liquid).[46,47] In this way, the process of metal adsorption, nucleation, and growth on surfaces has been analyzed quantitatively by Unwin et al.[43] In other approaches, reduction of the metal ions has been achieved by a reducing agent present in solution or electrogenerated by the substrate such as a redox mediator[41] or more recently by direct electron transfer through redox enzymes.[48] Also, metal ion reduction has been obtained in unbiased copper and silver substrates by galvanic replacement.[49] In another strategy, UME is used to generate the reduced form of a reversible redox mediator that diffuses to the substrate and injects charge to reduce metallic species present in solution or embedded in a polymeric matrix.[50]

All these strategies have different requirements and limitations. For example, the success of the formation of specific surface patterns depends on the generation of a continuous flux of metal ions and the ability of keeping constant a very small probe−substrate distance during scanning, thus allowing the diffusion of metal ions to the surface instead to the solution bulk.[37−40] It is also necessary to maintain acidic conditions to avoid the formation of metal oxides during the anodic dissolution of the microelectrode. For nonconducting surfaces, the experimental conditions must

Received: July 15, 2013
Revised: September 26, 2013
Published: September 26, 2013

   dx.doi.org/10.1021/jp406980b | J. Phys. Chem. C 2013, 117, 22087−22093

avoid oxidation of the reducing agent at the SECM tip while at the same time allowing the anodic generation of the metal ions.[41]

This paper reports an alternative and simple way for patterning gold surfaces with AuNPs using SECM by taking into account the considerations mentioned above. In contrast with previous methods,[21−43] the approach developed here is based on the "in situ" electrosynthesis of AuNPs by electrochemical reduction of a gold salt at a platinum ultramicroelectrode positioned on top of an unbiased gold surface modified with a biphenyl dithiol self-assembled monolayer (SAM). The synthesized AuNPs are chemisorbed on the thiolated SAM present at the gold surface (Figure 1). By shifting the microelectrode position across the thiol-modified surface while applying to it a reduction potential, particle-like lines can be generated at the surface.

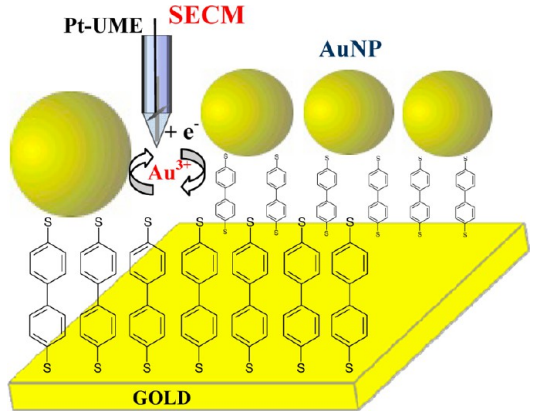

Figure 1. Schematic drawing of gold nanoparticle patterning of a gold surface modified with a SAM of biphenyl-4,4′-dithiol by SECM. AuNPs are electrosynthesized at the tip by electrochemical reduction of chloroaureate ions and attached by chemisorption to the thiolated SAM. The structures are not drawn to scale.

EXPERIMENTAL METHODS

Chemicals. Potassium hexachloroiridate(IV) technical grade, phenol (99%), hydrogen tetrachloroaurate(III) trihydrate (≥99.9% trace metals basis), and biphenyl-4,4′-dithiol were obtained from Sigma-Aldrich and used as received. Water was purified with a Millipore Milli-Q system. All solutions were prepared just prior to use.

UMEs Preparation. A pipet puller (PE-21, Narishige group) was used for UMEs preparation. An approximately 20 mm long 25 μm diameter Pt wire (Alfa Aesar, 99,95%) was inserted into a 100 mm long glass capillary with an outer diameter of 1.2 mm and an inner diameter of 0.68 mm in such a way that the Pt wire was located in the middle part of the capillary. The glass capillary was placed at the center of the heater in the puller chamber. The following values served for adjusting the heater level and the magnet level to produce the preferred electrodes: heater: 50; submagnet: 10; main magnet: 100. Using this method, each capillary−microwire section produces two needle-shaped electrodes. Electrical connection to the inside end of the Pt wire to a copper wire was made with silver epoxy.

Scanning Electrochemical Microscopy. SECM measurements were carried out with a CH Instruments model 900B SECM placed on a homemade antivibration table. The electrochemical cell was located on a *XYZ* positioning stage, and the distance between the tip and the sample was controlled using a stepper motor (coarse approach) combined with a piezoelectric nanopositioning system (fine approach, *X*, *Y*, *Z* resolution: 1.6 nm, Newport 423 series). All voltammetry and SECM measurements were performed in a grounded Faraday cage using a three-electrode configuration formed by a platinum wire auxiliary electrode, Ag/AgCl saturated reference electrode, and the fabricated Pt ultramicroelectrode.

The sample substrates were glass slides (1.1 cm × 1.1 cm) covered with evaporated gold layers (0.2−0.3 μm) deposited over a chromium adhesion layer (Gold Arrandee) suitable for flame annealing to obtain Au(111) terraces. Prior to use, the gold surfaces were cleaned by exposure to "piranha" solution (3:1 concentrated H_2SO_4/30% H_2O_2) followed by exhaustive rinsing with distilled water. *Caution: piranha solution reacts violently with most organic materials and may result in explosion or skin burns if not handled with extreme caution.* The gold surfaces were subsequently annealed for 2 min in a gas flame.

SAM-Functionalized Gold Substrates Preparation. Gold substrates were immersed for 24 h at room temperature in a 1 mM solution of biphenyl-4,4′-dithiol (Sigma-Aldrich) in absolute ethanol (HPLC grade, Sigma-Aldrich). The electrodes were subsequently rinsed with ethanol and dried in nitrogen.

Scanning Electron Microscopy (SEM). SEM imaging was carried out with a field emission-scanning electron microscope FE-SEM FEI Nova NANOSEM 230.

RESULTS AND DISCUSSION

A difficulty in patterning on rough surfaces or large areas is that the probe can crash and be damaged. To circumvent this, a flexible Pt tip like a fiber was used in a similar way to previously reported for carbon ultramicroelectrodes (UMEs).[51] On approaching the modified surface, the tip can establish a soft physical contact between probe apex and sample and remained the active electrode area at a given distance. For this purpose, Pt UMEs fabricated by heating and pulling a 25 μm Pt microwire inserted into a borosilicate glass capillary were employed. As the glass is drawn out, the Pt thins out and drastically reduces the radius of the wire, thus providing a close-fitting seal between the glass and the metal wire inside it. The Pt UMEs thus produced showed hemispherical shape as observed by optical and scanning electron microscopy and were electrochemically characterized by their voltammetric response for the reduction of 1 mM K_2IrCl_6 in 0.1 M KCl. Figure S1 shows a fully retraceable and well-shaped sigmoidal curve corresponding to the reduction of Ir(IV) to Ir(III) with a flat diffusion plateau, typical of UMEs.

From the steady-state limiting current, i_{lim} = 1.2 nA, and assuming a hemispherical geometry, a radius of 2.4 μm was calculated for the electrochemical active surface from[30,31,52−56]

$$i_{lim} = 2\pi nFDC^* r_{app} \quad (1)$$

where C^* and D are the bulk concentration (1 mM) and diffusion coefficient ($(8.2 \pm 0.4) \times 10^{-6}$ cm^2 s^{-1})[57] of $IrCl_6^{2-}$, respectively, r_{app} is the apparent radius of the exposed section of the tip, n is the number of electrons transferred per ion reduced (in this case n = 1), and F is Faraday's constant. Values of r_{app} are apparent values because they are based on an assumed geometry and an assumed mode of transport. Although at the simplest level the tip electrode can be approximated as a true hemisphere embedded in insulating plane of infinite area, the

dx.doi.org/10.1021/jp406980b | J. Phys. Chem. C 2013, 117, 22087−22093

exposed tip can also appear to be either a flattened hemispheroidal or a coneshaped electrode surrounded by a finite insulating sheath. For those geometries, analytical equations for the diffusion-limited current have been also described.[58−61] However, on the basis of the comparisons between them, it has been previously concluded that the current is insufficiently sensitive to the precise geometry to allow subtle differences in geometry to be determined by voltammetric measurements.[61] Therefore, eq 1 can be considered useful in providing a rough estimation of the exposed surface area of the electrodes since the hemispherical model for data analysis has been reported to be within the limits of acceptable experimental error.[60]

The electrochemical generation of AuNPs involves the reduction of $AuCl_4^-$ at the tip electrode. This process occurs through a nucleation and growth mechanism and was investigated at the UME tip by cyclic voltammetry. Typical cyclic voltammograms are shown in Figure 2. A characteristic

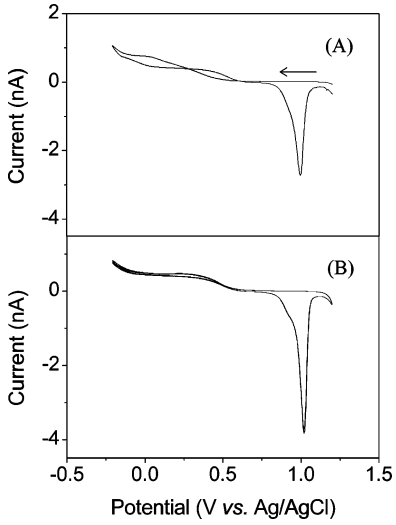

Figure 2. Cyclic voltammograms of a 2.4 μm radius Pt UME in 0.1 mM $HAuCl_4$ and 0.1 M KCl at a scan rate of 100 mV/s: (A) first scan; (B) second and third scans.

nucleation and growth loop is observed (Figure 2A) at potentials more negative than 0.4 V. The hysteresis observed disappears on successive scans since particle growth occurs on the nuclei remaining on the electrode surface (Figure 2B). The anodic stripping peak due to the dissolution of the gold deposited through the formation of a gold chloride complex is observed at 1.02 V. The stripping current in the second and successive scans is higher than that for the first, indicating increasing gold electrodeposition after nucleation.

The amount of gold electrodeposited on the Pt microelectrode estimated from the charge under the oxidation peak was 16.6×10^{-9} mol cm^{-2}. From these results an electrode growth potential of −0.2 V vs Ag/AgCl was chosen for the electrosynthesis of AuNPs so that the electrochemical reduction of gold ions took place under diffusion control.

A key issue for predicting particle size is the electrodeposition time; this was estimated by equating the hemispherical diffusion current to the charge according to[62]

$$2\pi nFDC^*r_{app} = (nFd_{Au}/M_{Au})(dV_{Au}/dt) = nFd_{Au} 2\pi r^2{}_{app}(dr_{app}/dt)/M_{Au} \quad (2)$$

where V_{Au} is the volume of the Au nanoparticle, d_{Au} is the density of Au, and M_{Au} is the molar mass of Au. Hence, for an applied potential supporting diffusion-limited current, the time-dependent deposition current conditions and nanoparticle radius for N gold particles growing in isolation are given by[63]

$$i(t) = \pi nFN((2DC^*)^3 M_{Au} t/d_{Au})^{1/2} \quad (3)$$

$$r(t) = (2DC^* M_{Au} t/d_{Au})^{1/2} \quad (4)$$

From eq 4 and taking $D_{Au(III)} = 1.0 \times 10^{-5}$ cm^2 s^{-1} calculated from the diffusion-limited current in Figure S1 (this value is in agreement with that reported in the literature[64,65]), an electrodeposition time of 0.1 s would yield 15 nm radius particles. This electrodeposition time was chosen to carry out the AuNPs patterning of the gold surface modified with a self-assembled monolayer (SAM) of biphenyl-4,4′-dithiol (see experimental details, Supporting Information). To achieve particle deposition on the target substrate, the tip−sample distance must be kept very close to the metal surface to make sure that the SECM tip is placed within the range of interaction between them.

For this the tip was approached to the surface using first a coarse approach and then a fine piezoelectric control approach before scanning the surface.

Figure S2A shows the normalized current $I_T = i_T/i_{T,\infty}$ as a function of the normalized distance $L = d/r_{app}$ for the approach curve tracking the electrochemical reduction of K_2IrCl_6 recorded with a slow approach rate of the tip to the sample surface. When the tip was positioned at a relatively long distance from the surface, $d > 10r_{app}$, a steady-state current, $i_{T,\infty}$, was rapidly established due to hemispherical diffusion of $IrCl_6^{2-}$ (Figure S2B, Supporting Information). This current remained constant at 1.2 nA with very low electrochemical noise until the tip reached the vicinity of the SAM-modified gold surface, where diffusion to the ultramicroelectrode was hindered and the steady-state current, i_T, gradually decreased compared with $i_{T,\infty}$. Electron transfer through the biphenyl-SAM indicates negative feedback behavior but with a still observable charge transfer. When the tip hit the gold surface, as indicated by a steep increase in current, it was immediately retracted ∼0.1 μm and once more approached very slowly to the surface (Figure S2B, Supporting Information). The current started again to decrease, and the approach was stopped this time in the onset of the enhanced current flow as indicative of the beginning of a physical contact of the tip with the surface. It should be noted that although a flexible tip is used, which can bend and flex in contact with the surface, in order to avoid tip crash and resulting sample damage after landing, the slowest tip approach speed and rate allowed are employed. However, we are aware of what the control of the tip−substrate distance at that nanometer-per-minute level is affected by mechanical and thermal drift due to expansion and contraction of components of SECM stage associated with temperature changes.[66−68]

Once the distance between tip and substrate was adjusted, a solution of $HAuCl_4$ was injected to the cell to obtain a concentration of 0.1 mM while simultaneously having present the Ir complex in the medium. The SECM tip was then moved in the $X-Y$ direction at a speed of 0.8 mm s^{-1} following a parallel line pattern with the lines spaced 20 μm. Nanoparticle electrosynthesis along the X-direction was carried out by stopping the tip every 0.02 s for 0.1 s while the potential was held at −0.2 V.

dx.doi.org/10.1021/jp406980b | J. Phys. Chem. C 2013, 117, 22087−22093

Figures 3 and 4 show the SEM images of the substrate obtained after this electrochemical procedure, revealing the

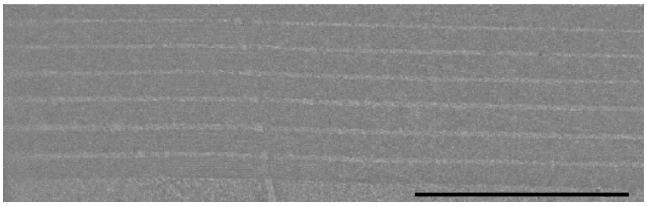

Figure 3. SEM image of the patterning of micrometer-sized lines of AuNPs over a gold surface following potential electrodeposition for 0.1 s at −0.2 V in the presence of 0.1 mM of $HAuCl_4$ using a SECM tip of ∼4.8 μm of diameter. Scale bar = 200 μm.

patterning of micrometer-sized lines separated by a distance of approximately 20 μm. The width of each line was approximately 2.3 μm, smaller than the diameter of the microelectrode employed, which can be associated with the tip area close enough to the gold surface for tip−substrate particle transfer. It is noteworthy that scraping the tip along the surface is not observed, confirming the soft of the physical contact between both during the transfer process.

In a zoomed image (Figure 4C) it is possible to distinguish that every line was formed mostly by Au nanoparticles densely and homogeneously distributed along the line some of them grouped forming assemblies. Nanoparticle distribution obtained from this image is shown in Figure S3 (Supporting Information). The average nanoparticle diameter is 32 ± 7 nm, which is in agreement with that expected from the above calculations for an electrodeposition time of 0.1 s considering gold particles growing in isolation. It seems to indicate that the two requirements for the formation of dimensionally uniform metal particles, instantaneous nucleation and diffusion-controlled growth, were both satisfied for the electrodeposition of metal particles of this size. In the image the electrodeposition of smaller and larger particles is also observed, the latter presumably formed by particle sintering due to Oswald ripening or particle coalescence. In this way, the single most important mechanism of distribution broadening for the growth of randomly nucleated metal particles on electrode surfaces has been explained in terms of "interparticle diffusion coupling" between particles.[69−71] It has been reported that the growth for individual metal particles on the surface depends on the number and proximity of neighboring particles. Under conditions of diffusion-controlled growth, a rapid enough depletion of reactant occurs at the particle surface, establishing a depletion layer surrounding each particle.[69] When two particles are enough close, their depletion layers can overlap, giving rise to a slower growth. This dispersion in the growth rates of individual particles on the surface leads to smaller particles than that expected.

The size of the nanoparticles and the width of the patterned line can be altered either by varying the electrodeposition time or the radius of the UME employed. Figure 5 shows thinner deposition lines obtained by decreasing the tip size and increasing the electrodeposition time to 1s. In this case, the width was ∼700 nm, but the line became partially metalized due to the sintering of the nanoparticles (Figure 5B) as a consequence of a major gold deposition.

It is proposed that the formation of the lines occurs as follows: gold atoms formed can nucleate and grow either on the

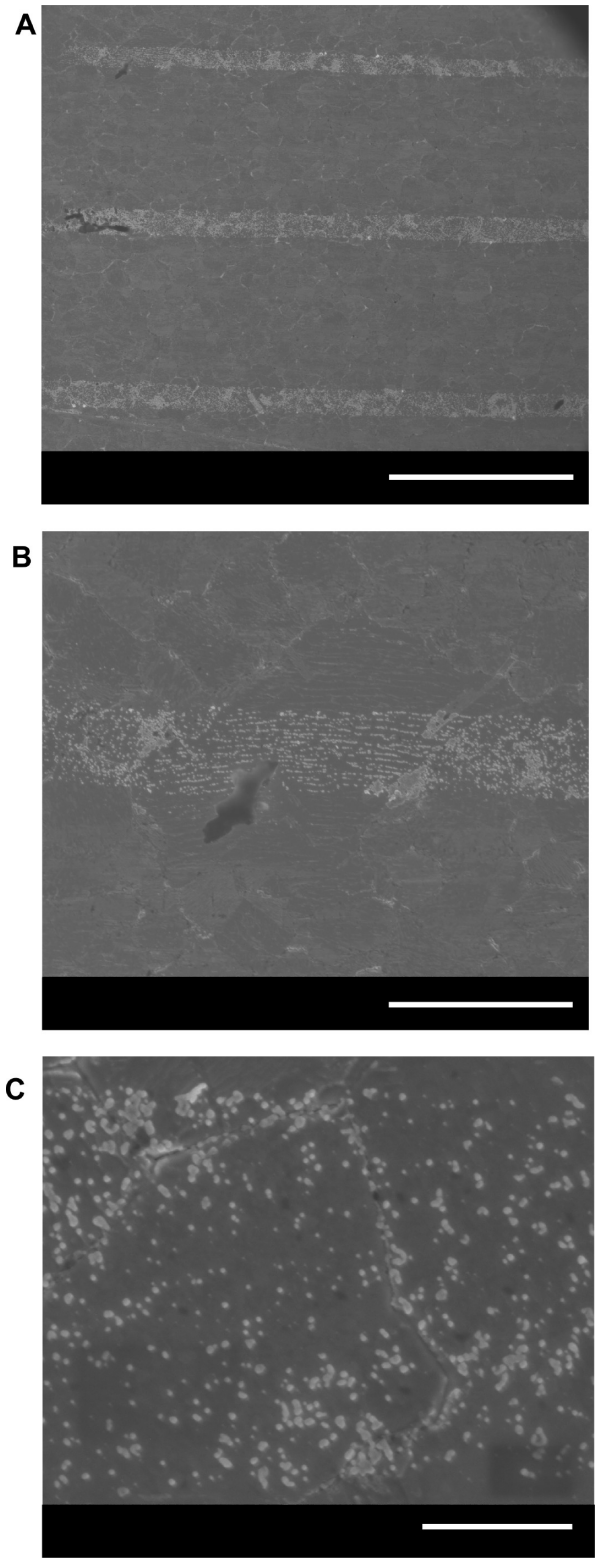

Figure 4. SEM images at different magnifications of the patterning of micrometer-sized lines of AuNPs over a gold surface modified with a SAM of biphenyl-4,4′-dithiol following potential electrodeposition for 0.1 s at −0.2 V in the presence of 0.1 mM of $HAuCl_4$ using a SECM tip of ∼4.8 μm of diameter. Scale bars correspond to 20, 5, and 1 μm, respectively.

Pt-tip electrode itself or at sites on the SAM modified surface. In the first case, as the amount of gold and therefore the size of nanoparticle formed increase, the contact between the tip and

dx.doi.org/10.1021/jp406980b | J. Phys. Chem. C 2013, 117, 22087−22093

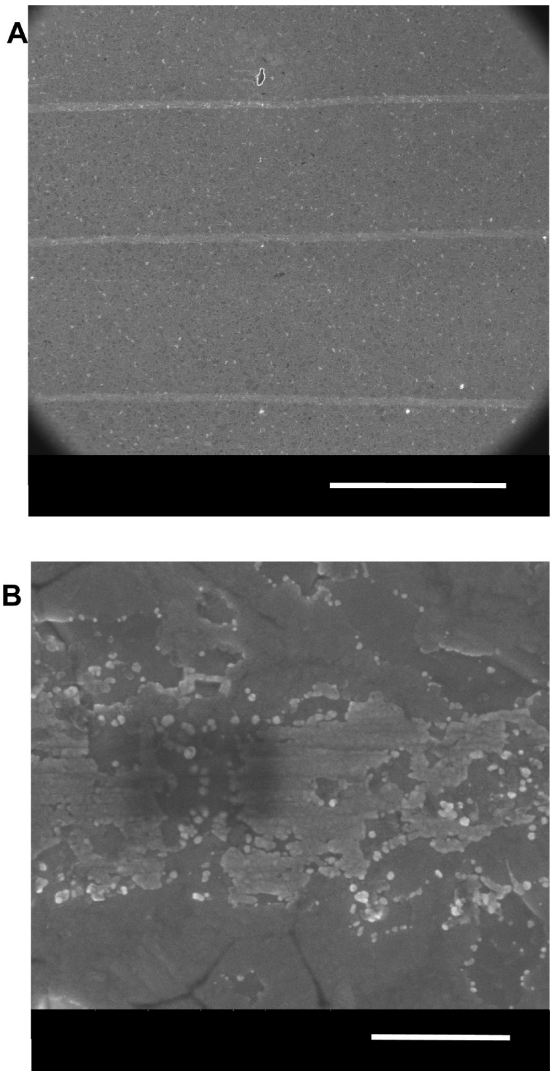

Figure 5. SEM images at different magnifications of the patterning of micrometer-sized lines of AuNPs over a gold surface modified with a SAM of biphenyl-4,4′-dithiol following potential electrodeposition for 1 s at −0.2 V in the presence of 0.1 mM $HAuCl_4$ using a SECM tip of ∼1.5 μm diameter. Scale bars correspond to 20 μm and 500 nm, respectively.

the particle becomes weak compared with the forces that are established between the nanoparticle and the thiol groups in the SAM.[32] Thus, when the tip is moved across the SAM modified surface after the electrodeposition cycle, the contact between the tip and the nanoparticle is broken, giving rise to the attachment of the particle onto the thiol-modified surface. Thus, binding of the nanoparticles formed to the thiol groups on the substrate provides the required adhesion to the substrate.

Control experiments carried out in similar conditions as described above, but in the absence of gold salt did not result in the formation and deposition of any particle (Figure S4, Supporting Information). On the contrary, experiments performed on a bare gold surface without thiol-SAM gave rise to the deposition of some particles randomly distributed across the surface presumable attached by Au−Au interactions (Figure S5, Supporting Information). However, no particle-like lines were observed, thus providing clear evidence about the key role of the SAM in the patterning process.

CONCLUSIONS

To summarize, patterned arrays of gold nanoparticles can be fabricated by direct electrosynthesis and deposition using SECM in a simple way. Flexible UMEs were employed to minimize the possibility of tip crashing onto the surface, thus allowing its precise approach. This work opens the possibility of using this technique for patterning different types of particle-like patterns on different surfaces including nonconductive substrates since biasing the surface is not required.

ASSOCIATED CONTENT

Supporting Information

Electrochemical characterization of Pt ultramicroelectrodes; approach curves of Pt-UME toward a thiol-modified gold surface; particle size distribution estimated from SEM image in Figure 4C; SEM images obtained after patterning of micrometer-sized lines following potential electrodeposition on a gold surface modified with a SAM of biphenyl-4,4′-dithiol in the absence of $HAuCl_4$ and on a bare gold surface in the presence of $HAuCl_4$. This material is available free of charge via the Internet at http://pubs.acs.org.

AUTHOR INFORMATION

Corresponding Author

*E-mail josemaria.abad@uam.es; Tel +34914978467 (J.M.A.).

Present Address

[§]A.Y.T.: INQUIMAE, Facultad de Ciencias Exactas y Naturales, Pabellón 2, Ciudad Universitaria, AR-1428 Buenos Aires, Argentina.

Notes

The authors declare no competing financial interest.

ACKNOWLEDGMENTS

This work has been supported by DGUI of Comunidad Autónoma de Madrid (CAM) and UAM (project No. CCG10-UAM/MAT-5731), Spanish Ministerio de Ciencia e Innovación (project No. CTQ2011-28157), and by CAM (project No. S2009/PPQ-1642, AVANSENS). J.M.A. acknowledges research funding by a "Ramon y Cajal" contract from the Spanish Ministry of Science and Innovation. A.Y.T. acknowledges a fellowship from CONICET and Fundación Carolina. We are grateful to Tech. Andrés Valera (ICMM-CSIC) for carrying out SEM measurements and Dr. Elena Casero (UAM) for supporting in the use of SECM instrumentation. The authors also thank Prof. D. J. Schiffrin (University of Liverpool) and Dr. Edmund Leary (IMDEA-Nanociencia) for comments on this manuscript.

REFERENCES

(1) Ono, L. K.; Cuenya, B. R. Formation and Thermal Stability of Au_2O_3 on Gold Nanoparticles: Size and Support Effects. *J. Phys. Chem. C* **2008**, *112*, 4676−4686.

(2) Stratakis, M.; Garcia, H. Catalysis by Supported Gold Nanoparticles: Beyond Aerobic Oxidative Processes. *Chem. Rev.* **2012**, *112*, 4469−4506.

(3) Covington, E.; Bohrer, F. I.; Xu, C.; Zellers, E. T.; Kurdak, Ç. Densely Integrated Array of Chemiresistor Vapor Sensors with Electron-Beam Patterned Monolayer-Protected Gold Nanoparticle Interface Films. *Lab Chip* **2010**, *10*, 3058−3060.

(4) Menard, E.; Meitl, M. A.; Sun, Y.; Park, J.; Shir, D. J.; Nam, Y. S.; Jeon, S.; Rogers, J. A. Micro- and Nanopatterning Techniques for Organic Electronic and Optoelectronic Systems. *Chem. Rev.* **2007**, *107*, 1117−1160.

(5) Shipway, A. N.; Katz, E.; Willner, I. Nanoparticle Arrays on Surfaces for Electronic, Optical, and Sensor Applications. *ChemPhysChem* **2000**, *1*, 18−52.
(6) Daniel, M. C.; Astruc, D. Gold Nanoparticles: Assembly, Supramolecular Chemistry, Quantum-Size-Related Properties, and Applications toward Biology, Catalysis and Nanotechnology. *Chem. Rev.* **2004**, *104*, 293−346.
(7) Xia, Y.; Rogers, J. A.; Paul, K. E.; Whitesides, G. M. Unconventional Methods for Fabricating and Patterning Nanostructures. *Chem. Rev.* **1999**, *99*, 1823−1848.
(8) Lu, N.; Gleiche, M.; Zheng, J.; Lenhert, S.; Xu, B.; Chi, L.; Fuchs, H. Fabrication of Chemically Patterned Surfaces Based on Template-Directed Self-Assembly. *Adv. Mater.* **2002**, *14*, 1812−1815.
(9) Foster, E.; Kearns, G.; Goto, S.; Hutchison, J. E. Patterned Gold-Nanoparticle Monolayers Assembled on the Oxide of Silicon. *Adv. Mater.* **2005**, *17*, 1542−1545.
(10) Xia, D.; Brueck, S. R. J. A Facile Approach to Directed Assembly of Patterns of Nanoparticles Using Interference Lithography and Spin Coating. *Nano Lett.* **2004**, *4*, 1295−1299.
(11) Subramani, C.; Dickert, S.; Yeh, Y.-C.; Tuominen, M. T.; Rotello, V. M. Supramolecular Functionalization of Electron-Beam Generated Nanostructures. *Langmuir* **2011**, *27*, 1543−1545.
(12) Werts, M. H. V.; Lambert, M.; Bourgoin, J.-P.; Brust, M. Nanometer Scale Patterning of Langmuir−Blodgett Films of Gold Nanoparticles by Electron Beam Lithography. *Nano Lett.* **2002**, *2*, 43−47.
(13) Corbierre, M. K.; Beerens, J.; Lennox, R. B. Gold Nanoparticles Generated by Electron Beam Lithography of Gold(I)−Thiolate Thin Films. *Chem. Mater.* **2005**, *17*, 5774−5779.
(14) Mendes, P. M.; Jacke, S.; Critchley, K.; Plaza, J.; Chen, Y.; Nikitin, K.; Palmer, R. E.; Evans, S. D.; Fitzmaurice, D. Gold Nanoparticle Patterning of Silicon Wafers Using Chemical e-Beam Lithography. *Langmuir* **2004**, *20*, 3766−3768.
(15) Liu, X.; Fu, L.; Hong, S.; Dravid, V. P.; Mirkin, C. A. Arrays of Magnetic Nanoparticles Patterned via "Dip-Pen" Nanolithography. *Adv. Mater.* **2002**, *14*, 231−234.
(16) Braunschweig, A. B.; Senesi, A. J.; Mirkin, C. A. Redox-Activating Dip-Pen Nanolithography (RA-DPN). *J. Am. Chem. Soc.* **2009**, *131*, 922−923.
(17) Piner, R. D.; Zhu, J.; Xu, F.; Hong, S. H.; Mirkin, C. A. "Dip-Pen" Nanolithography. *Science* **1999**, *283*, 661−663.
(18) Xia, Y. N.; Whitesides, G. M. Use of Controlled Reactive Spreading of Liquid Alkanethiol on the Surface of Gold to Modify the Size of Features Produced by Microcontact Printing. *J. Am. Chem. Soc.* **1995**, *117*, 3274−3275.
(19) Rozkiewicz, D. I.; Janczewski, D.; Verboom, W.; Ravoo, B. J.; Reinhoudt, D. N. "Click" Chemistry by Microcontact Printing. *Angew. Chem., Int. Ed.* **2006**, *45*, 5292−5296.
(20) Yu, X.; Pham, J. T.; Subramani, C.; Creran, B.; Yeh, Y.-C.; Du, K.; Patra, D.; Miranda, O. R.; Crosby, A. J.; Rotello, V. M. Direct Patterning of Engineered Ionic Gold Nanoparticles via Nanoimprint Lithography. *Adv. Mater.* **2012**, *24*, 6330−6334.
(21) Li, Q.; Zheng, J. W.; Liu, Z. F. Site-Selective Assemblies of Gold Nanoparticles on an AFM Tip-Defined Silicon Template. *Langmuir* **2003**, *19*, 166−171.
(22) Krämer, S.; Fuierer, R. R.; Gorman, C. B. Scanning Probe Lithography Using Self-Assembled Monolayers. *Chem. Rev.* **2003**, *103*, 4367−4418.
(23) Eigler, D. M.; Schweizer, E. K. Positioning Single Atoms with a Scanning Tunnelling Microscope. *Nature* **1990**, *344*, 524−526.
(24) Liu, S.; Schmid, G.; Maoz, R.; Sagiv, J. Template Guided Self-Assembly of [Au_{55}] Clusters on Nanolithographically Defined Monolayer Patterns. *Nano Lett.* **2002**, *2*, 1055−1060.
(25) Chowdhury, D.; Maoz, R.; Sagiv, J. Wetting Driven Self-Assembly as a New Approach to Template-Guided Fabrication of Metal Nanopatterns. *Nano Lett.* **2007**, *7*, 1770−1778.
(26) Zheng, H.; Lee, I.; Rubner, M. F.; Hammond, P. T. Two Component Particle Arrays on Patterned Polyelectrolyte Multilayer Templates. *Adv. Mater.* **2002**, *14*, 569−572.
(27) Liu, S.; Maoz, R.; Sagiv, J. Planned Nanostructures of Colloidal Gold via Self-Assembly on Hierarchically Assembled Organic Bilayer Template Patterns with In-Situ Generated Terminal Amino Functionality. *Nano Lett.* **2004**, *4*, 845−851.
(28) Nyffenegger, R. M.; Penner, R. M. Nanometer-Scale Surface Modification Using the Scanning Probe Microscope: Progress Since 1991. *Chem. Rev.* **1997**, *97*, 1195−1230.
(29) Zhao, J.; Terfort, A.; Zharnikov, M. Gold Nanoparticle Patterning on Monomolecular Chemical Templates Fabricated by Irradiation-Promoted Exchange Reaction. *J. Phys. Chem. C* **2011**, *115*, 14058−14066.
(30) Mandler, D. Micro- and Nanopatterning Using the Scanning Electrochemical Microscope. In *Scanning Electrochemical Microscopy*; Bard, A. J., Mirkin, M. V., Eds.; Marcel Dekker: New York, 2001; pp 593−627.
(31) Wittstock, G.; Burchardt, M.; Pust, S. E.; Shen, Y.; Zhao, C. Scanning Electrochemical Microscopy for Direct Imaging of Reaction Rates. *Angew. Chem., Int. Ed.* **2007**, *46*, 1584−1617.
(32) Hüisser, O. E.; Craston, D. H.; Bard, A. J. Scanning Electrochemical Microscopy: High-Resolution Deposition and Etching of Metals. *J. Electrochem. Soc.* **1989**, *136*, 3222−3229.
(33) Mandler, D.; Bard, A. J. A New Approach to the High Resolution Electrodeposition of Metals via the Feedback Mode of the Scanning Electrochemical Microscope. *J. Electrochem. Soc.* **1990**, *137*, 1079−1086.
(34) Borgwarth, K.; Heinze, J. Increasing the Resolution of the Scanning Electrochemical Microscope Using a Chemical Lens: Application to Silver Deposition. *J. Electrochem. Soc.* **1999**, *146*, 3285−3289.
(35) Heβ, C.; Borgwarth, K.; Ricken, C.; Ebling, D. G.; Heinze, J. Scanning Electrochemical Microscopy: Study of Silver Deposition on Non-Conducting Substrates. *Electrochim. Acta* **1997**, *42*, 3065−3073.
(36) Forouzan, F.; Bard, A. J. Evidence for Faradaic Processes in Scanning Probe Microscopy on Mica in Humid Air. *J. Phys. Chem. B* **1997**, *101*, 10876−10879.
(37) Meltzer, S.; Mandler, D. Microwriting of Gold Patterns with the Scanning Electrochemical Microscope. *J. Electrochem. Soc.* **1995**, *142*, L82−L84.
(38) Turyan, I.; Matsue, T.; Mandler, D. Patterning and Characterization of Surfaces with Organic and Biological Molecules by the Scanning Electrochemical Microscope. *Anal. Chem.* **2000**, *72*, 3431−3435.
(39) Ammann, E.; Mandler, D. Local Deposition of Gold on Silicon by the Scanning Electrochemical Microscope. *J. Electrochem. Soc.* **2001**, *148*, C533−C539.
(40) Sheffer, M.; Mandler, D. Control of Locally Deposited Gold Nanoparticle on Polyaniline Films. *Electrochim. Acta* **2009**, *54*, 2951−2956.
(41) Malel, E.; Mandler, D. Localized Electroless Deposition of Gold Nanoparticles Using Scanning Electrochemical Microscopy Electrochemical/Chemical Deposition and Etching. *J. Electrochem. Soc.* **2008**, *155*, D459−D467.
(42) Meltzer, S.; Mandler, D. Study of Silicon Etching in HBr Solutions Using a Scanning Electrochemical Microscope. *J. Chem. Soc., Faraday Trans.* **1995**, *91*, 1019−1024.
(43) Unwin, P. R.; Macpherson, J. V.; Martin, R. D.; McConville, C. F. Scanning Electrochemical Microscopy as a Dynamic Probe of Metal Adsorption, Nucleation and Growth on Surfaces: Silver Deposition on Pyrite. In *Localised In-Situ Methods for Investigating Electrochemical Interfaces*; Electrochemical Society Proceedings Vol. *99-28*; Taylor, S. R., Hillier, A. C., Seo, M., Eds.; Electrochemical Society: Pennington, NJ, 1999; pp 104−121.
(44) Malel, E.; Colleran, J.; Mandler, D. Studying the Localized Deposition of Ag Nanoparticles on Self-Assembled Monolayers by Scanning Electrochemical Microscopy (SECM). *Electrochim. Acta* **2011**, *56*, 6954−6961.
(45) De Abril, O.; Mandler, D.; Unwin, P. R. Local Cobalt Electrodeposition Using the Scanning Electrochemical Microscope. *Electrochem. Solid-State Lett.* **2004**, *7*, C71−C74.

(46) Li, F.; Edwards, M.; Guo, J.; Unwin, P. R. Silver Particle Nucleation and Growth at Liquid/Liquid Interfaces: A Scanning Electrochemical Microscopy Approach. *J. Phys. Chem. C* **2009**, *113*, 3553−3565.
(47) Yatziv, Y.; Turyan, I.; Mandler, D. A New Approach to Micropatterning: Application of Potential-Assisted Ion Transfer at the Liquid−Liquid Interface for the Local Metal Deposition. *J. Am. Chem. Soc.* **2002**, *124*, 5618−5619.
(48) Malel, E.; Ludwig, R.; Gorton, L.; Mandler, D. Localized Deposition of Au Nanoparticles by Direct Electron Transfer Through Cellobiose Dehydrogenase. *Chem.—Eur. J.* **2010**, *16*, 11697−11706.
(49) O'Mullane, A. P.; Ippolito, S. J.; Bond, A. M.; Bhargava, S. K. A Study of Localised Galvanic Replacement of Copper and Silver Films with Gold Using Scanning Electrochemical Microscopy. *Electrochem. Commun.* **2010**, *12*, 611−615.
(50) Combellas, C.; Kanoufi, F.; Mazouzi, D.; Thiebault, A. Surface Modification of Halogenated Polymers: 5. Localized Electroless Deposition of Metals on Poly(tetrafluoroethylene) Surfaces. *J. Electroanal. Chem.* **2003**, *556*, 43−52.
(51) Cortes Salazar, F.; Momotenko, D.; Girault, H.; Lesch, A.; Wittstock, G. Seeing Big with Scanning Electrochemical Microscopy. *Anal. Chem.* **2011**, *83*, 1493−1499.
(52) Penner, R. M.; Heben, M. J.; Longin, T. L.; Lewis, N. S. Fabrication and Use of Nanometer-Sized Electrodes in Electrochemistry. *Science* **1990**, *250*, 1118−1121.
(53) Penner, R. M.; Heben, M. J.; Lewis, N. J. Preparation and Electrochemical Characterization of Conical and Hemispherical Ultramicroelectrodes. *Anal. Chem.* **1989**, *61*, 1630−1636.
(54) Slevin, C. J.; Gray, N. J.; Macpherson, J. V.; Webb, M. A.; Unwin, P. R. Fabrication and Characterisation of Nanometre-Sized Platinum Electrodes for Voltammetric Analysis and Imaging. *Electrochem. Commun.* **1999**, *1*, 282−288.
(55) Macpherson, J. V.; Unwin, P. R. Combined Scanning Electrochemical−Atomic Force Microscopy. *Anal. Chem.* **2000**, *72*, 276−285.
(56) Conyers, J. L., Jr.; White, H. S. Electrochemical Characterization of Electrodes with Submicrometer Dimensions. *Anal. Chem.* **2000**, *72*, 4441−4446.
(57) Llopis, J. F.; Colom, F. In *Encyclopedia of Electrochemistry of the Elements*; Bard, A. J., Ed.; Marcel Dekker Inc.: New York, 1976; Vol. *6*, pp 224−226.
(58) Fang, Y.; Leddy, J. Cyclic Voltammetric Responses for Inlaid Microdisks with Shields of Thickness Comparable to the Electrode Radius: A Simulation of Reversible Electrode Kinetics. *Anal. Chem.* **1995**, *67*, 1259−1270.
(59) Myland, J. C.; Oldham, K. B. Diffusion-Limited Currents at Hemispheroidal Microelectrodes. *J. Electroanal. Chem.* **1990**, *288*, 1−14.
(60) Zoski, C. G.; Mirkin, M. V. Steady-State Limiting Currents at Finite Conical Microelectrodes. *Anal. Chem.* **2002**, *74*, 1986−1992.
(61) Watkins, J. J.; Chen, J. Y.; White, H. S.; Abruña, H. D.; Maisonhaute, E.; Amatore, C. Zeptomole Voltammetric Detection and Electron-Transfer Rate Measurements Using Platinum Electrodes of Nanometer Dimensions. *Anal. Chem.* **2003**, *75*, 3962−3971.
(62) Tel-Vered, R.; Bard, A. J. Generation and Detection of Single Metal Nanoparticles Using Scanning Electrochemical Microscopy Techniques. *J. Phys. Chem. B* **2006**, *110*, 25279−25287.
(63) Bobbert, P. A.; Wind, M. M.; Vlieger, J. *Physica A* **1987**, *146*, 69.
(64) Cheh, H. Y. Electrodeposition of Gold by Pulsed Current. *J. Electrochem. Soc.* **1971**, *118*, 551−557.
(65) Segal, C. C.; Chase, A. B.; Young, A. M. High Field Pulse Plating: Gold on Platinum Electrodes. *J. Electrochem. Soc.* **1992**, *139*, 1580−1585.
(66) Kim, J.; Shen, M.; Nioradze, N.; Amemiya, S. Stabilizing Nanometer Scale Tip-to-Substrate Gaps in Scanning Electrochemical Microscopy Using an Isothermal Chamber for Thermal Drift Suppression. *Anal. Chem.* **2012**, *84*, 3489−3492.
(67) Moheimani, S. O. R. Accurate and Fast Nanopositioning with Piezoelectric Tube Scanners: Emerging Trends and Future Challenges. *Rev. Sci. Instrum.* **2008**, *79*, 071101.
(68) Marinello, F.; Balcon, M.; Schiavuta, P.; Carmignato, S.; Savio, E. Thermal Drift Study on Different Commercial Scanning Probe Microscopes during the Initial Warming-up Phase. *Meas. Sci. Technol.* **2011**, *22*, 094016.
(69) Penner, R. M. Mesoscopic Metal Particles and Wires by Electrodeposition. *J. Phys. Chem. B* **2002**, *106*, 3339−3353.
(70) Penner, R. M. Brownian Dynamics Simulations of the Growth of Metal Nanocrystal Ensembles on Electrode Surfaces in Solution: 2. The Effect of Deposition Rate on Particle Size Dispersion. *J. Phys. Chem. B* **2001**, *105*, 8672−8678.
(71) Zoval, J. V.; Lee, J.; Gorer, S.; Penner, R. M. Electrochemical Preparation of Platinum Nanocrystallites with Size Selectivity on Basal Plane Oriented Graphite Surfaces. *J. Phys. Chem. B* **1998**, *102*, 1166−1175.